Water Reuse

© 2023 The Authors

Water Reuse Vol 13 No 4, 525 doi: 10.2166/wrd.2023.050

Bi-LSTM and partial mutual information selection-based forecasting groundwater salinization levels

A. Muniappan[a], T. Jarin[b], R. Sabitha[c], Ayman A. Ghfar[d], I. M. Rizwanul Fattah[e], Chilala Kakoma Bowa[f] and Mabvuto Mwanza[g,*]

[a] Saveetha School of Engineering, Saveetha Institute of Medical and Technical Sciences, Chennai 602105, India
[b] Department of Electrical and Electronics Engineering, Jyothi Engineering College, Thrissur, India
[c] Department of CSE, Rajalakshmi Engineering College, Thandalam, Chennai, India
[d] Department of Chemistry, College of Science, King Saud University, P.O. Box 2455, Riyadh 11451, Saudi Arabia
[e] Centre for Technology in Water and Wastewater, School of Civil and Environmental Engineering, Faculty of Engineering and IT, University of Technology Sydney, Sydney, Australia
[f] Department of Strategy & Planning, Rural Electrification Authority, Lusaka, Zambia
[g] Department of Electrical & Electronic Engineering, School of Engineering, University of Zambia, P.O. Box 32379, Lusaka, 10101, Zambia
*Corresponding author. E-mail: mabvuto.mwanza@unza.zm; mabvuto_mwanza@yahoo.com

CKB, 0000-0003-4902-2019; MM, 0000-0003-3764-9252

ABSTRACT

Fresh-saline groundwater is distributed in a highly heterogeneous way throughout the world. Groundwater salinization is a serious environmental issue that harms ecosystems and public health in coastal regions worldwide. Because of the complexities of groundwater salinization processes and the variables that influence them, it is challenging to predict groundwater salinity concentrations precisely. It compares cutting-edge machine learning (ML) algorithms for predicting groundwater salinity and identifying contributing factors. It employs bi-directional long short-term memory (BiLSTM) to indicate groundwater salinity. The input variable selection problem has attracted attention in the time series modeling community because it has been shown that information-theoretic input variable selection algorithms provide a more accurate representation of the modeled process than linear alternatives. To generate sample combinations for training multiple BiLSTM models, PMIS-selected predictors are used, and the predicted values from various BiLSTM models are also used to calculate the degree of prediction uncertainty for groundwater levels. The findings give policymakers insights for recommending groundwater salinity remediation and management strategies in the context of excessive groundwater exploitation in coastal lowland regions. To ensure sustainable groundwater management in coastal areas, it is essential to recognize the significant impact of human-caused factors on groundwater salinization.

Key words: bi-directional long short-term memory (BiLSTM), fresh-saline groundwater, groundwater, machine learning (ML), partial correlation input selection (PCIS), partial mutual information (PMI)

HIGHLIGHTS

- The purpose of this research is to compare cutting-edge machine learning (ML) algorithms for predicting groundwater salinity and identifying significant factors.
- The salinity of groundwater is indicated using bi-directional long short-term memory (BiLSTM) in this study.
- Diverse sample combinations for training multiple bi-directional long short-term memory (BiLSTM) models were generated using PMIS-selected predictors.

GRAPHICAL ABSTRACT

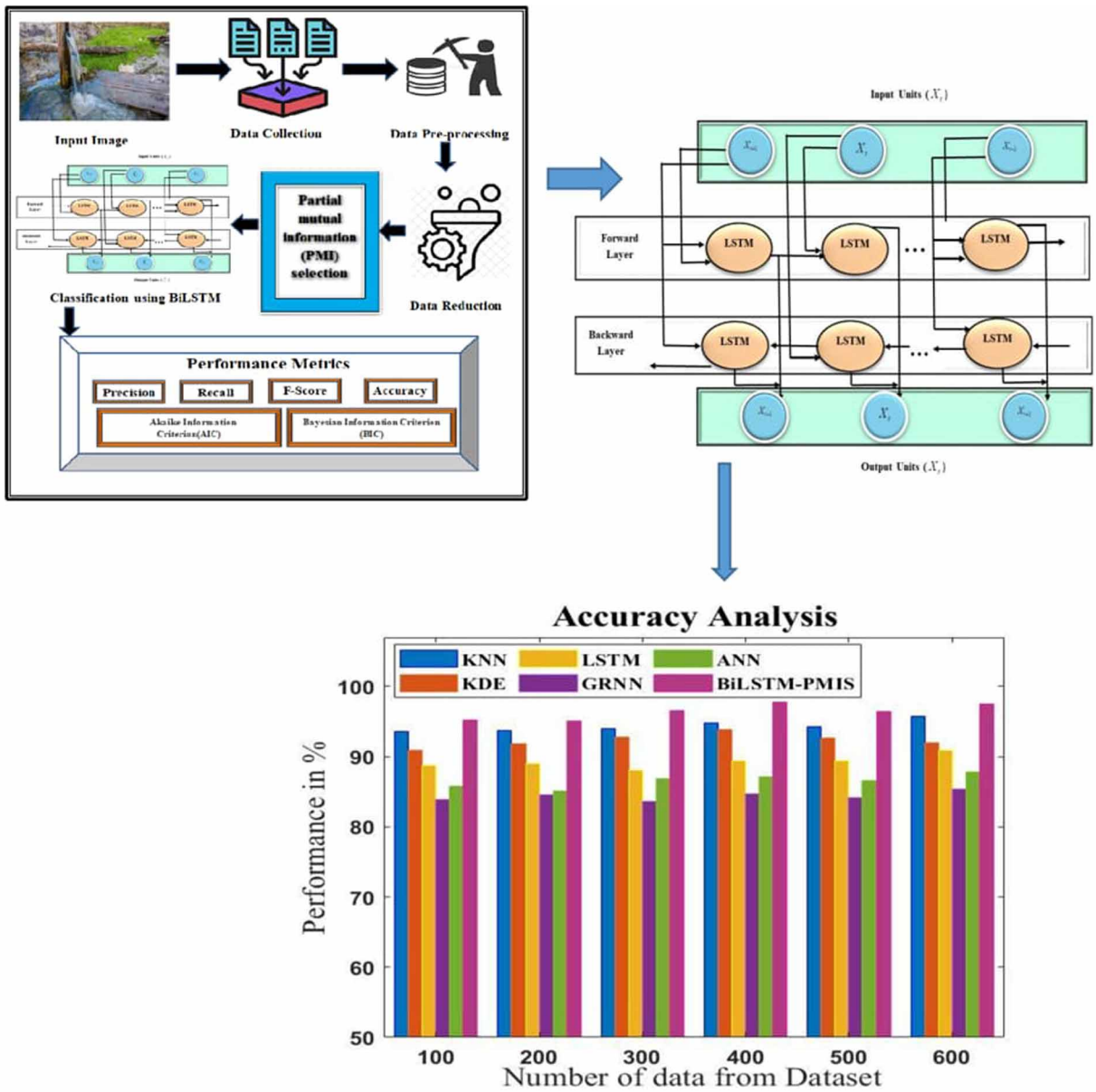

1. INTRODUCTION

Underground water is an essential natural source in various states worldwide. It survives in the voids of aquifers, which are earthen rock and soil formations. Groundwater is used for multiple purposes and requirements, including irrigation, industrial processes, the provision of drinking water and as a source of energy for water streams (Pourghasemi *et al.* 2020). Therefore, it is essential to keep an eye on the amount or number of groundwater resources to determine if there is any overuse or depletion. Measuring groundwater level (GWL), or the depth under the crushed external at which the earth or pillar is stable due to the presence of water, is the most accurate way to estimate the number of groundwater resources. Machine learning (ML) is being researched and developed to improve groundwater resource management. As a result, the world is changing, and many processes in various engineering fields are improving (Demirci *et al.* 2019).

Water is essential for life in the coastal zone. Still, its sufficient quantity and quality availability are threatened by various factors, including a changing climate, land subsidence, tourism, and agriculture. Climate change could have a considerable

impact on groundwater recharge rates in significant aquifer systems, which would also affect the availability of fresh groundwater supplies (Neumann *et al.* 2017). Rising sea levels in coastal aquifers exacerbate the effects of saltwater intrusion on water quality. Most at risk are shallow coastal aquifers. Rainfall increases due to climate change, increasing the capacity of coastal aquifer storage. The effects of geology, topography, and land use significantly influence groundwater recharge. The recharging rate of an unconfined aquifer can be affected (Post *et al.* 2018). Precipitation, rivers, and lakes all help with the process of recharging an unconfined aquifer.

Globally, deltaic coastal plains face various problems, including groundwater salinization, land subsidence, coastal erosion, depletion of available land, and environmentally risky land use practices. Because the holocene marine transgression was not entirely washed away by rain, many low-lying coastal regions have salty groundwater. The seepage or upwelling of saltwater from deeper formations or aquifers causes salinization (Antonellini *et al.* 2015).

Mediterranean coastal aquifers are vulnerable to saltwater intrusion due to their high hydraulic conductivity and wasting water during the summer. Two interconnected factors caused this. Because of rapid anthropogenic subsidence and artificial drainage, the unconfined and semiconfined aquifers along the Ravenna coast have become salinized (Colombani *et al.* 2015). The drainage system used for land reclamation creates a vertical gradient that pushes groundwater upward and regulates the groundwater table. From the deepest part of the aquifer, it is possible to mobilize and transport connate salty groundwater upward. Drainage lowers aquifer recharge. The coastal water table is generally at or below sea level, and drainage impacts the hydraulic gradient directed inland (Cozzolino *et al.* 2017).

Land subsidence negatively affects coastal groundwater resources, as well as the availability of freshwater, because of sinking topography. The shallow unconfined aquifer's water table has risen due to subsidence, requiring more mechanical pumping (Giambastiani *et al.* 2020). There is more water to drain if there is more subsidence. The system slows as less freshwater can replenish the aquifer. A few freshwater lenses exist in the coastal aquifer near Ravenna, but most are brackish to saline. Over the past century, salinization has increased, endangering the ecosystems in this area. The coastal aquifer is a closed system that receives its only recharge from rain or intensive irrigation in dune regions and other locations where sandy deposits are exposed: low rainfall and high evaporation all limit aquifer infiltration. Seawater encroaches on rivers and canals because there are no sea barriers, causing salinization. The nearby aquifer, which joins surface and groundwater, may become salted by the salt pools at the river's bottom (Choubin & Malekian 2017).

Statistical models are suitable substitutes when there is a lack of data, and the accuracy of forecasts is valued over comprehension of underlying mechanisms (Daliakopoulos *et al.* 2005). An autoregressive moving average (ARMA) model, for instance, was created by Bidwell (2005) to anticipate groundwater levels in New Zealand. The groundwater level (GWL) was predicted using a similar ARMA model in a study by Lee *et al.* (2009) in Changwon, Korea. In a different research, Guzman *et al.* (2017) used an artificial neural network (ANN) model to replicate daily GWL at a smaller scale in the southeast U.S. Mississippi River Valley Alluvial Aquifer. By employing bioinspired adaptive neuro-fuzzy inference system (ANFIS) models, Yaseen *et al.* (2019) attempted to estimate the highly nonlinear streamflow of the Pahang River.

However, the models above frequently encounter difficulties when working with nonstationary data and can only handle such data after first preparing the input. Finding methods for handling nonstationary data more successfully takes more effort because the techniques are less mature than those for handling static data. Wavelet analysis is an illustration of one such approach.

Long short-term memory (LSTM) is a growing study area, although bi-directional long short-term memory (BiLSTM) applications for more complex natural data are still uncommon. The original aspect of the current study is creating a novel layer structure for BiLSTM-based models that uses the sequence-to-one module for complex biological phenomena like GWL fluctuations. To the best of the authors' knowledge, the most recent investigations were restricted to using a module of sequence-to-sequence regression under a straightforward deep neural networks (DNNs) model architecture to predict GWL fluctuations. The authors' unique proposed models have yet to be the subject of any research studies published in the literature. One benefit of the proposed BiLSTM models is that they do not need a significant amount of hydrological and meteorological variable records as essential input data for modeling, unlike the costly, challenging, and time-consuming module of sequence-to-sequence regression.

For the daily GWL forecast and uncertainty, this work suggests BiLSTM paired with PMIS, and it tests its application in various climate zones. The following are the paper's objectives:

(1) To determine significant predictors for GWLs in each of the various climate zones

(2) To evaluate the predictions with ML models and establish the best BiLSTM model structure and parameter values
(3) To employ PMIS and BiLSTM combined to assess the prediction uncertainty.

This paper's remaining sections are as follows: Our BiLSTM-partial mutual information (PMI) algorithm's theoretical underpinnings are provided in Section 2, while the various variable input selection algorithms are explained in Unit 3, the practical consequences are covered in Unit 4, and our main conclusions and recommendations for more study are provided in Section 5.

2. LITERATURE SURVEY

Sahoo & Jha (2015) used multiple linear regression (MLR) to forecast groundwater levels in unconfined aquifers. This study's findings demonstrated the importance of MLR models as a low-cost and straightforward GWL modeling tool when sufficient data were unavailable. MLR models could predict GWLs with an acceptable level of accuracy. An issue with MLR is that it needs to handle input and output nonlinearity. This nonlinearity is typical in physical-based models.

The study by Yousefi *et al.* (2019) used MATLAB to forecast Karaj's GWL. They conducted their analysis for over 10 years. Optimistic, pessimistic, and continuing scenarios were all modeled using GWL. Unconfined groundwater flow issues were improved using the stand-alone program MODFLOW2005-NWT. The complexity of groundwater level (GWL) forecasting is due to the numerous limitations in accurately representing the mental processes of the groundwater scheme.

According to the research by Mohammadi (Mosavi *et al.* 2021b), it was highlighted that due to their ability to adjust to new data and build on prior calculations to produce precise predictions, ML techniques are becoming increasingly popular. For this reason, ML techniques are crucial for mapping groundwater salinity and hardness susceptibility making ML models more dependable.

Huang *et al.* (2017) predicted GWLs in China using an ANN, SVM, and M5 T and compared their findings. The M5 T model performed the best during testing. Models were run using daily meteorological and hydrological data. Due to the high correlation, all three models produced usable results. The models, however, require addition models to predict peak events accurately.

Models like Artificial Neural Networks (ANN) and Artificial Neural Networks-Particle Swarm Optimization (ANNPSO) utilize hybrid artificial intelligence by integrating various algorithms (Maroufpoor *et al.* 2020). Inverse distance weighting, radial basis function, and kriging are three geostatistical representations the researchers used to compare hybrid models. After carefully examining the representations and computing electrical conductivity (EC), sodium absorption ratio (SAR), and Cl, it was concluded that the neuro-fuzzy-grid partition (NF-GP) model is the most effective for assessing groundwater value in shafts.

Iqbal *et al.* (2020) created a model to forecast daily GWL in Pakistan utilizing an ANN. Several inputs were used: Raf, T_{max}, T_{min}, maximum and minimum temperatures, solar radiation, percentage, wind speed (WS), area elevation, and polygon area. The authors used a variety of ANN constructions, each with its particular transmission purposes, hidden layers, and data proportions, throughout the training, validation, and testing phases to select the most accurate prediction model for groundwater level (GWL). Levenberg–Marquardt (LM) back-propagation was used to facilitate learning. The education found that the suggested perfect gave a precise estimation of GWL compared to statistical criteria. The tangent sigmoid transmission purpose was the most effective transfer function, and the most effective information split was 80% training, 10% validation, and 10% challenging.

Chen *et al.* (2020) compared the results of simulating GWL with a finite difference numerical model to those obtained using ANNs and SVM. Overall, the ML models outperformed the numerical model. The finite difference method was superior because it could generalize, including the aquifer's physical mechanism.

Artificial neural networks (ANNs) were used by Sunayana *et al.* (2020) in their study to predict the water quality at a landfill. The researchers used three algorithms to train various models, allowing them to choose the best strategy for precise predictions. They employed several elements in the input layer, including pH, TDS, chlorides Cl, NO_3, and SO_4^2, but just one in the production layer: total hardness. The parameters that have the most significant impact on total hardness were found using examination sensitivity. They used ArcGIS to create a map to assess the capability of an LSTM (Vu *et al.* 2020). Over 50 years, it gathered GWL data from 31 piezometers. Correlation coefficients of 0.64–0.99 and root-mean-square errors (RMSE) of 0.07–1.05 m demonstrate the feasibility of deep learning for reconstructing GWL fluctuations. Sun *et al.* (2019) combined deep understanding with NASA's NOAH land surface model to progress the groundwater storing forecast in India. This study improved groundwater forecasting. The GRACE and NOAH groundwater mismatches are learned using a convolutional neural networks (CNN) model.

Nie *et al.* (2017) worked with RBF-NN and RBF-SVM to forecast the once-a-month GWL in Jilin, China. The radial basis function (RBF) kernel purpose had to be programmed to configure the SVM model structure. The input and output measurement errors were the basis for the calculated uncertainties. To quantify this uncertainty, 95% confidence intervals were used. The RBF-SVM model outperformed the RBF-NN model when forecasting monthly GWL fluctuations.

The NARX-ANN and RBF-SVR models that were created were utilized to evaluate the groundwater levels (GWL) in Mississippi irrigation wells (Guzman *et al.* 2019). The analysis used polynomial, radial basis, and sigmoid kernel functions to identify the SVR model with the slightest training error. The accuracy was highest while using the RBF kernel function. The researchers divided historical time into winter and summer, or 'withdrawal' and 'recharging,' respectively. RBF-SVR generated more precise seasonal forecasts than NARX-ANN (summer or winter). GWL predictions by season were additional more accurate than predictions utilizing the complete period sequence. The linear nature of the winter season's problem reduced the computation time required by the RBF-SVR model.

For estimating monthly GWL in four Tunisian aquifers, Nouri and Malek (Derbela & Nouiri 2020) advanced an ANN perfect. Models for forecasting in Africa were developed using Raf, GWL, and ethno-veterinary practices (EVP). The ANN model captured the dynamic piezometric fluctuations and produced more accurate forecasts. According to the study, monthly precipitation, EVP, and previous GWL values affect monthly GWL.

In the research conducted by Shamsuddin *et al.* (2017) for Jenderam Hilir, Selangor Malaysia, the forecasts for the daily GWL were produced using the Multilayer Perceptron (MLP) model. The decision to use ANN structures was driven by their potential to enhance estimation performance. These structures were chosen based on meteorological and hydrological factors. The predictive models were trained using LM. According to statistical criteria, MLR has proven to be a valuable technique for estimating GWL. A notable correlation existed between GWL and hydrological parameters.

To forecast regular GWL fluctuations in an Indian microcomputer watershed, Javadinejad *et al.* (2020) developed the MLP-NN and M5-MT representations. Between 1996 and 2006, monthly GWL values from a Ganjimatta well were gathered to achieve this objective. Two case studies were conducted to assess the MLP-NN model's input combinations. Based on these hypotheses, the MLP-NN model predictors are the current and 1-month-lagged GWL, T, and Raf values. The best input combinations were identified by the researchers using linear rules. As a result, M5-MT was developed. The predicted values were contrasted with the observed values using R^2, RMSE, NSE, and RE. When indicating changes to the GWL, the MLP-NN model lagged behind the M5-MT model.

Maps of water quality and water tables help with water resource management. Streams, rivers, lakes, and ponds all affect the groundwater table. When drawing maps of the water table and quality, all of this must be considered. Various hydrological and geological factors, water table, riverbed geometry, and substratum hydrogeology limitations influence surface water and groundwater interactions. Despite the many studies and factors that affect coastal aquifer salinization, a regional spatial analysis that considers the water table level and groundwater electrical conductivity has yet to be performed in the study area. In this kind of analysis, surface water features are also considered.

To forecast groundwater salinity and identify the variables that affect it, the most recent ML algorithms were evaluated. BiLSTM is utilized in this study to forecast groundwater salinity. Interest in time series modeling, particularly in water resource applications, has recently increased due to the choice of input variables. Because there is evidence that nonlinear information-theoretic algorithms, like partial mutual info (PMI) assortment (PMIS), model the process more accurately than linear alternatives, like partial correlation input selection (PCIS), the problem of variable input selection has attracted the attention of time series modelers (PCIS). Modeling water resources with nonlinear input variables is a popular application of the PMIS algorithm. To train numerous BiLSTM models, PMIS selects predictors to create sample combinations. The findings can aid in developing management and remediation plans for coastal lowlands' excessive groundwater exploitation. Groundwater has become significantly salinized due to human activity, necessitating immediate action.

This thorough review examines the relevant literature and offers a concise and insightful analysis across several crucial areas. This review covers a variety of subjects, such as the methods used to collect groundwater, regional groundwater modeling, physicochemical analysis, spatial variation in quality parameters, use of Geographic Information System (GIS), and ML techniques to predict groundwater parameter values, and analysis of the water's suitability for drinking and irrigation. Pre- and post-monsoon periods are used for hydrogeochemical analysis, water quality index analysis, and statistical techniques to forecast the quality decline of groundwater. To increase the prediction performance of BiLSTM-PMIS approaches, pre-processing tools are utilized at the beginning of the calibration procedure.

3. PROPOSED SYSTEM

3.1. The Palestinian Water Authority

In 1995, the Palestinian Water Power was created by President Yasser Arafat's Decree No. 90 (PWA). The goal of the Water Authority is to accomplish integration. Incomplete water possessions must be maintained, protected, and preserved within the confines of legal frameworks that allow the authority to achieve a healthy environment in instruction to confirm a balance between the quantity and superiority of easily accessible water and the needs of the Palestinian people for maintainable expansion through aquatic properties. These goals are to be achieved by carrying out the subsequent tasks: Protection and preservation of those resources within the framework of legal frameworks that enable the authority to achieve a healthy state; management of limited water resources that are integrated and sustainable; Ample supplies of wholesome food and water should be present.

3.2. Data collection and acquisition

The historical salinity data from three Deir El-Balah wells for this study (S-69, K-20, and K-21) were randomly gathered from the PWA. Salinity readings from 1989 are found on S-69, while lessons from 2000 are located on K-20 and K-21. That identified the relevant tables and columns for our research and the set of the subsequent stage. The research by Al Jami *et al.* (2020) and Sharafati *et al.* (2020) created the GWL information set for small-diameter wells to display GWL. The J-103 and S-50 wells were selected from the GWL dataset. The water level in 1973 is shown on S-50, while the water level in 1971 is on J-103. The BiLSTM-PMI method is shown schematically in Figures 1 and 2.

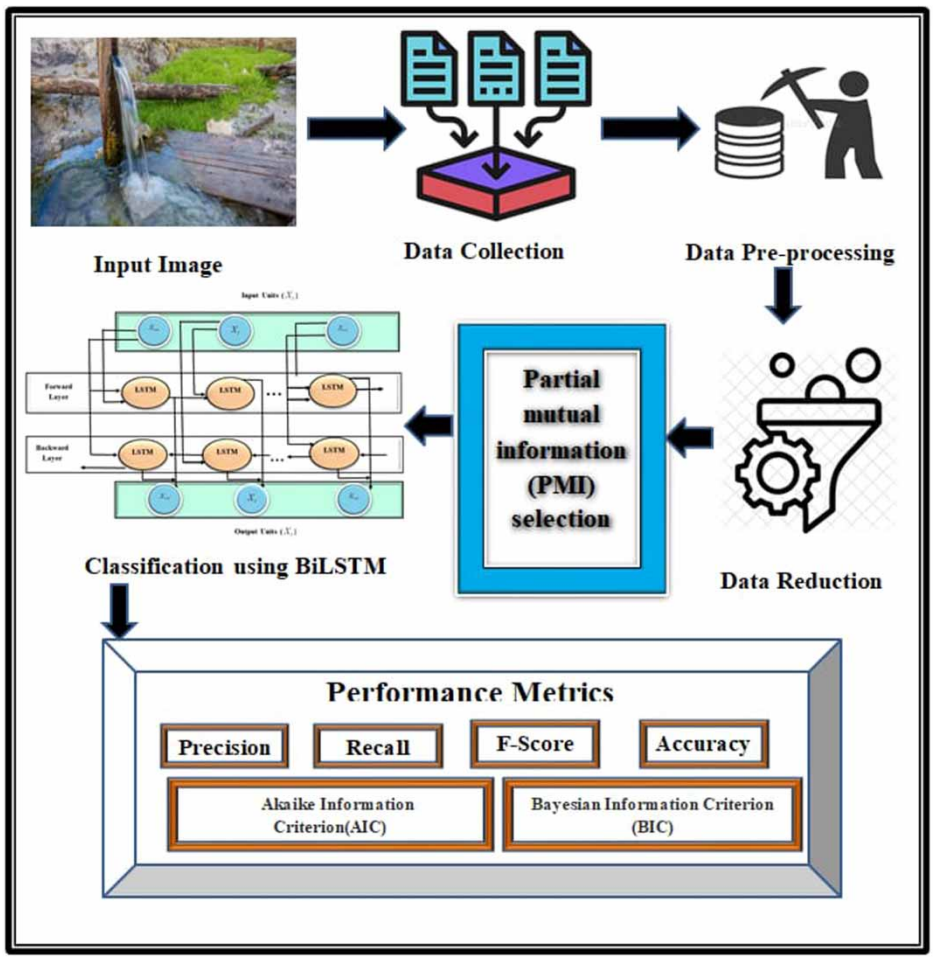

Figure 1 | The proposed technique of BiLSTM-PMIS.

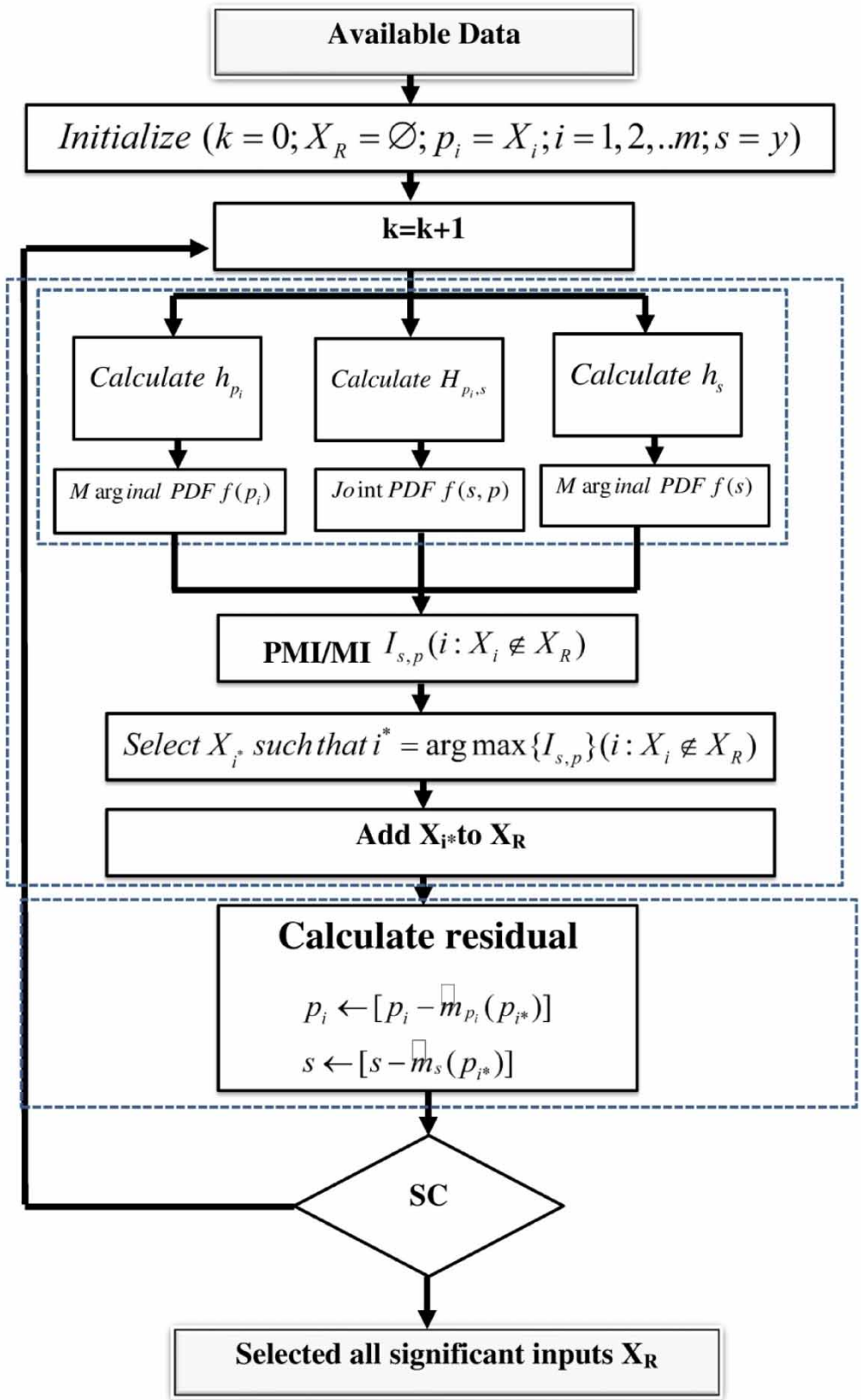

Figure 2 | The PMI procedure used in this study (the superscript d is omitted because all operations are performed on the input data $j = 1, 2, ..n$).

3.3. Data pre-processing

Several pre-processing tasks must be finished before they could use the forecasting algorithms. The pre-processing with Microsoft Excel 2016 includes the steps listed below, which are covered in more detail below.

3.4. Data reduction

The GWL and salinity rates datasets were reduced to eliminate all unnecessary attributes. Three wells in the city of Deir El-Balah, selected randomly, were connected to the datasets. As shown in Table 1, each of these wells that were part of a dataset was established as a time series. Table 2 depicts the additional established GWL data. 'Date' represents time, and 'WL' signifies sound water level (the value of WL grounds takes three belongings, either negative, positive, or equal to zero). Negative numbers indicate that the water level in the well is lower than in the sea, while positive numbers indicate the opposite. Salt may contaminate nearby groundwater production wells if the water level in the checking bores drops.

3.5. PMI-based input selection algorithm

The data-driven approach used by the BiLSTM modeling technique has been previously discussed. In cases where accurately formulating relationships among contributions and productions is problematic or implausible, this modeling approach has advantages over actual-based modeling. Developing data-driven forecasting and prediction models includes a crucial step called input selection. PMI selection-based forecasting in groundwater modeling has diverse applications, ranging from short-term prediction of groundwater levels to long-term assessments of climate change impacts. It helps understand the complex interactions between groundwater and various influencing factors, aiding in sustainable water resource management, environmental protection, and decision-making processes. PMI selection model applications include GWL prediction, drought and flood forecasting, groundwater contamination prediction, and climate change impact assessment.

GWL prediction often involves analyzing and understanding the relationships between various hydrological factors that can influence groundwater levels. PMI can capture direct and indirect dependencies between variables, making it suitable for identifying the most relevant features related to groundwater levels. Groundwater systems can exhibit complex and nonlinear behaviors due to rainfall patterns, geological properties, and human interventions. PMI effectively detects and quantifies nonlinear relationships between variables, allowing for the exploration of complex ways and dependencies within the data. When the underlying linearity hypothesis is valid, the statistical analysis based on partial association and

Table 1 | Precision analysis for BiLSTM-PMIS method with existing systems

No of data from dataset	KNN	KDE	LSTM	GRNN	ANN	BiLSTM-PMIS
100	86.562	88.527	91.265	94.736	96.725	97.753
200	87.973	88.927	90.763	93.925	96.325	97.526
300	86.536	88.324	91.728	94.535	95.042	96.426
400	86.076	88.064	90.937	94.435	95.426	96.826
500	87.552	88.626	91.627	93.766	95.826	96.982
600	86.536	89.852	91.853	93.625	96.224	96.057

GRNN, general regression neural network; KNN, K-nearest neighbors.

Table 2 | Recall analysis for BiLSTM-PMIS method with existing systems

No of data from dataset	KNN	KDE	LSTM	GRNN	ANN	BiLSTM-PMIS
100	83.763	84.526	85.938	88.735	89.735	94.838
200	83.863	84.322	85.435	88.634	89.636	94.865
300	83.082	84.937	86.045	88.437	90.645	96.652
400	83.535	85.736	87.634	88.836	91.336	96.043
500	83.635	86.937	87.935	89.907	92.453	95.453
600	83.974	86.736	87.735	88.943	92.836	97.735

connection used to choose input variables is useful. Sharma proposed a PMI-based collection procedure (PMSI), which Bowden and May subsequently created and applied. Assuming linearity when dealing with nonlinear modeling was avoided by doing this (Sadat-Noori *et al.* 2020; Prakash *et al.* 2022). The algorithm for selecting inputs using PMI is described below.

(a) Considering previous knowledge, the modeler's experience, and other pertinent factors like data accessibility, identifies potential input candidates for the model.
(b) The prospective set C and the chosen input variable set S require preliminary work.
(c) Subtract from the residuals of the output u and residuals of the applicant variables the residuals of the current inputs. As a result, you can calculate the output u's residual.

$$s = Y - E[y|X = x] \tag{1}$$

$$p = Z - E[z|X = x] \tag{2}$$

where s: preliminary value, p: probability density, y: result of selected input.

Y stands for the result, X for all the selected inputs, and Z for all the unselected inputs up to this point. The restricted hope E of y based on $X = x$ is calculated using a kernel function, a non-parametric deterioration technique. There is a calculation done. The estimation is based on what follows:

$$E[y|X = x] = \frac{\sum_{i=1}^{n} y_i K_h(x - x_i)}{\sum_{i=1}^{n} K_h(x - x_i)} \tag{3}$$

where K: kernel density.
where n means the overall number of observations, and x_i signifies the number of statements included in a sample. The fourth step additionally comprises

(d) determining the candidate with the highest potential by calculating mutual information $I(p, s)$ and I for the third variable

$$I(p, s) \approx \frac{1}{n}\sum_{i=1}^{n} \log\left[\frac{f(p_i, s_i)}{f(p_i)f(s_i)}\right] \tag{4}$$

where the marginal probability densities are $f(p_i)$ and $f(s_i)$, and $f(p_i, s_i)$ is the joint probability density. The marginal and joint probability densities are calculated using kernel density estimation (KDE). The probability density estimator is depicted for a given x position.

$$\widehat{f}(x) = \frac{1}{n}\sum_{i=1}^{n} K_h(x - x_i) \tag{5}$$

In stages (c), the subsequent Gaussian kernel is utilized (d).

$$K_h = \frac{1}{\left(\sqrt{2\pi h}\right)^d \sqrt{|\sigma|}} \exp\left(-\frac{(x - x_i)^T \sigma^{-1}(x - x_i)}{2h^2}\right) \tag{6}$$

where h stands for the kernel's bandwidth, r for an example covariance matrix, and d for the size of the chosen inputs. The subsequent formulation is used to compute the Gaussian reference bandwidth h_r:

$$h_r = \left(\frac{4}{d+2}\right)^{1/(d+4)} n^{-1/(d+4)} \tag{7}$$

The kernel bandwidth is h.

$$h = sf.h_r \tag{8}$$

sf is the climbing influence. This variable determines the amount of kernel smoothing. Mutual information estimates are consistent with a $\approx 1.5\,h_r$ bandwidth.

Step 1 established the worth of a particular termination criterion (e), compared some conclusion criteria and recommended that real-world applications use the Akaike information criterion (AIC). The AIC calculation entails:

$$\mathrm{AIC} = nIn\left(\frac{1}{n}\sum_{i=1}^{n} s_i^2\right) + 2p \tag{9}$$

If adding the candidate chosen in step (d) causes the AIC to decrease (f), transfer the candidate to S in step (e), where p denotes the total amount of model limitations used. If the AIC does not go down, the selection procedure can be completed or resumed by going back to step (c).

PCIS, or partial correlation-based contribution assortment, is a method for selecting inputs similar to PMIS. In PMIS stages (c) and (d), PCIS calculates residual and partial correlation in place of non-parametric recession and mutual information. PCIS uses MLR, linear correlation, and linear methods to calculate the residual and partial correlation. The linear correlation is computed using a variety of linear techniques. PCIS that can be helped in the proposed model BiLSTM are: (i) data pre-processing is gathering historical data of groundwater levels and potential input variables, such as precipitation, temperature, soil moisture, and groundwater recharge. Ensure that the data are adequately cleaned and formatted. (ii) Feature selection – calculate the partial correlation between each input variable and the GWL while controlling for the effects of other variables. This can be done using statistical methods such as the partial correlation coefficient or algorithms like the perturbed chain (PC) or fast incremental association rule mining (FIARM) algorithm. (iii) Select relevant features – identify the input variables with significant partial correlations with the GWL. These elements should be considered as inputs to the BiLSTM model since they will probably significantly impact ground level.

3.6. Classification BiLSTM

The behaviors that call for supervision were categorized in this section. As an alternative to Hidden Markov Modeling and other classification methods, a novel deep learning (DL) model was developed based on LSTM. These techniques are employed to classify data. This list includes both of these conventional classification systems (LSTM). The LSTM network, a subset of recurrent neural networks (RNNs), achieves this goal by accurately and effectively modeling sequential data. The essential structural elements of the LSTM network are graphically represented in Figure 3.

The LSTM model, a recursive model, solves the long-term dependency issue of a standard RNN. The accompanying diagram shows the input gates, memory cells, forget gates, and output gates that make up the LSTM model. The input gate

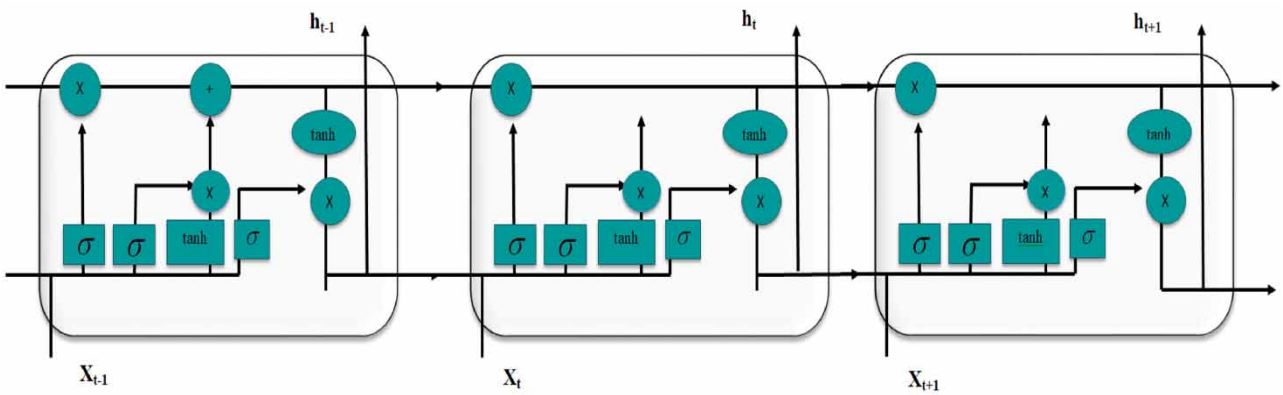

Figure 3 | The basic long short-term memory.

specifies information added to the cell state, the forget gate determines data deleted from the cell state, and the output gate selects information from the cell state. The storage unit's hidden layer contains the model's fundamental elements, and the gate structure has the power to alter or maintain the storage unit's state. The input x_t at the current time, the memory unit state $Ct-1$ from time $t1$, and the output $ht1$ from the storage unit from time $t1$ are the three information points each memory unit receives at time t. The output information points are the current output ht and unit state Ct. The internal structure of an LSTM memory unit at a specific time t and its relationship to the current state of neighboring temporal memory units are used to determine how accurately a single memory unit is calculated at time t.

The LSTM's 'cell' is where the state vector is stored. The data that are previously entered are summarized in the state vector. The most recent input and output data and data from earlier 'cells' are used to update the displayed state. To correct its shape, the LSTM network has a gate control mechanism that enables it to 'learn' the time stamp or 'forget' the initial cell state (Alotaibi *et al.* 2022; Metwally *et al.* 2022). The ability of LSTM networks to learn from their time stamps makes this possible. The cell state may sometimes be 'forgotten' by the network. The value of C_t, which symbolizes the memory cell's state at time step t, changes.

$$j_t = \sigma(V_{xj}x_t + V_{hj}h_{t-1} + b_j) \tag{10}$$

$$f_t = \sigma(V_{xf}x_t + V_{hf}h_{t-1} + b_f) \tag{11}$$

$$o_t = \sigma(V_{xo}x_t + V_{ho}h_{t-1} + b_o) \tag{12}$$

$$g_t = \tan h(V_{xc}x_t + V_{hc}h_{t-1} + b_c) \tag{13}$$

$$c_t = f_t \odot c_{t-1} + i_t \odot g_t \tag{14}$$

$$h_t = o_t \odot \tan h(c_t) \tag{15}$$

where σ is the given context's sigmoid function and $x \odot y$ is the element-wise product. For linear transformation, the version $V_{xi}, \ldots., V_{hc}$ includes weight matrices. b_j, b_f, b_o, b_c are the bias vectors. The Input gate, forget gate(ft), output gate(ot), state update(gt), and output hidden state vectors(ht) are all contained in this vector.

The input gate manages the information flow from the input and the forget gate f_t manages the information flow from the output. Remember that the gate control's behavior is also taught from data. Because of the recurrent nature of LSTM nodes, even if they only have one layer, these nodes can be combined to form 'deep' neural networks. The input gate manages the information flow from the input and the forget gate f_t manages information flow from the output. Remember that the gate control's behavior is also taught from data. A 'deep' neural network can consist of just one layer of LSTM nodes because of their recurrent nature. The availability of present and past contexts can improve a wide range of sequence classification tasks. Standard LSTM networks, on the other hand, process sequences in the order they occur in time and ignore contexts from earlier in the process. The hidden-to-hidden connections in the second layer of bi-directional LSTM (BiLSTM) networks flow in the reverse temporal order as in the first layer.

This enables standard LSTM networks to have a broader range of capabilities. As a result, the bi-directional model can use past and future data. The trajectory-based bi-directional LSTM model (BiLSTM) we developed during our research was used to classify and predict groundwater salinity levels.

The output from the two directions was combined using vector concatenation, resulting in twice as many outcomes for the layer that followed it. We added an output network to the hidden state to extract the data critical to the class labels. We used a softmax layer with a fully connected (FC) layer consisting of a linear transformation. The organizational structure of our network is shown in Figure 4.

An explanation of its features: road plane position data stored in trajectories must be transformed into sequential elements in the correct temporal order. Because they are sensitive to changes in groundwater salinization forecasting, general features like location coordinates can frequently contain noisy information. Because angular changes are more robust than other features, we used them to capture trajectory variations in our work. A variety of factors can contribute to these variations. Represent the trajectories of a forecasting groundwater salinization at the time step t, and let (x_{t+1}, y_{t+1}) represent the

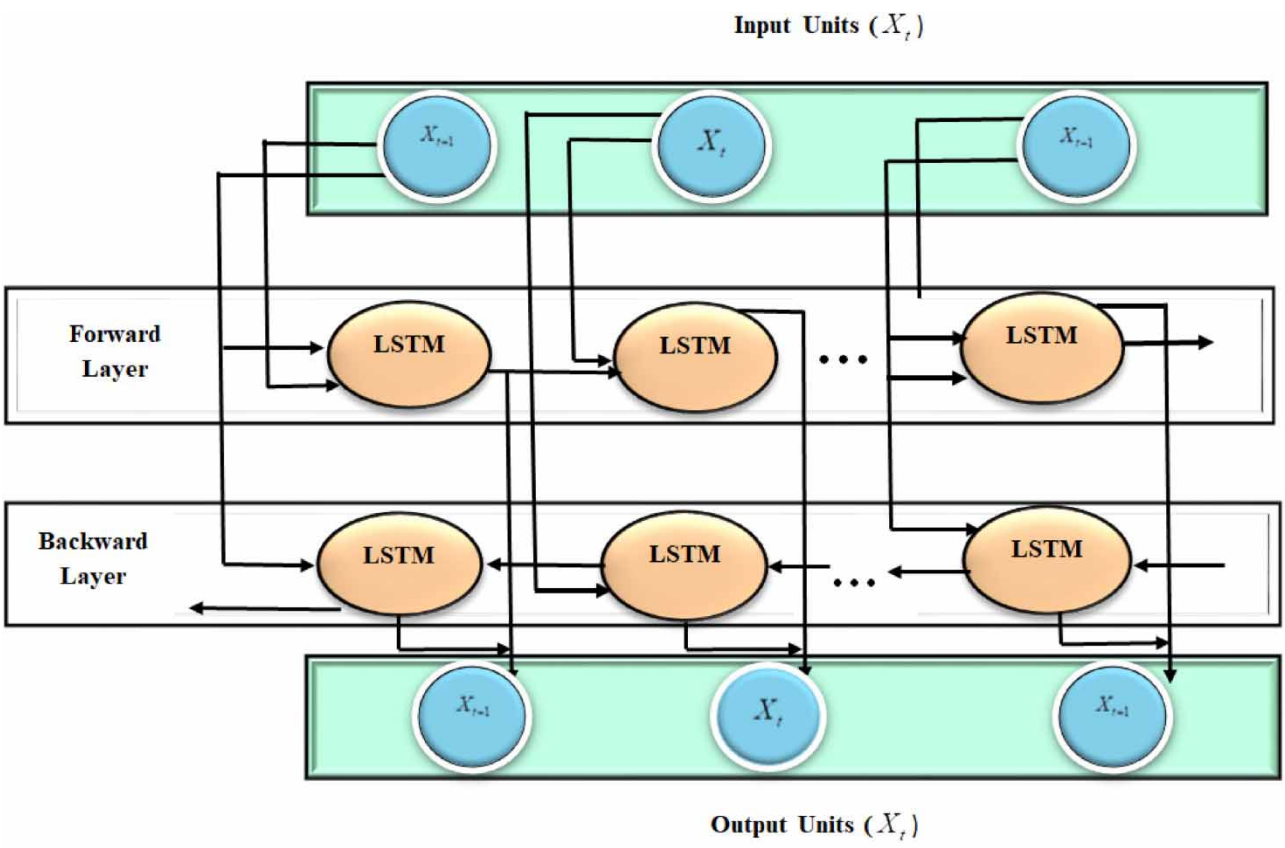

Figure 4 | Bilston is used in the trajectory classification network structure (BiLSTM).

trajectories at the time step $t + 1$. The following step is to compute the direction angle.

$$\theta = \arctan \frac{(y_{t+1} - y_t)}{(x_{t+1} - x_l)} \tag{16}$$

Training: we approached behavior recognition as a multi-class classification problem to predict one class label based on the sequential characteristics of a test used to forecast groundwater salinity levels. The BiLSTM was trained by reducing the negative log-likelihood function, denoted as follows:

$$L(v) = \sum_{I}^{t=1} \sum_{m=1}^{M} c_{t,m} In\, z_{t,m} + (1 - c_{t,m}) In(1 - z_{t,m}) + \lambda \Phi(v) \tag{17}$$

where v denotes the parameter of the neural network, I represents the number of training samples, $c_{t,m}$ is the mth entry of ct, z_{tm} is the mth output of the softmax layer and $\Phi(v)$ is the regularization term controlled by the λ.

4. RESULT AND DISCUSSION

4.1. Performance evaluation

The confusion matrix is used for accuracy, precision, recall, and *F*-score. A look at the *F*-score, memory, accuracy, and precision. The four binary classification metrics (positive/negative) are used. This includes false negatives (FN). Performance metrics that are essential for ML pipelines to function effectively are applied. The following are the statistical criteria to assess the proposed waste classification architecture and validate our suggested system:

Accuracy: The accuracy (Eq. (18)) metric shows how closely our predicted and actual values match. The proportion of true negatives and true positives to all possible discounts is used to express the study's findings.

$$\text{Accuracy} = \frac{\text{TP} + \text{TN}}{\text{TP} + \text{TN} + \text{FP} + \text{FN}} \tag{18}$$

Recall: It also goes by the name recall rate and actual positive rate. It determines the frequency at which a classifier correctly classifies a favorable result and then offers an assessment based on these results. It is specified by the following equation.

$$\text{Recall} = \frac{\text{TP}}{\text{TP} + \text{FN}} \tag{19}$$

Precision (Prec): this metric presents the percentage of appropriate classifications. Equation (20) can be used to represent it.

$$\text{Precision} = \frac{\text{TP}}{\text{TP} + \text{FP}} \tag{20}$$

F-measure (F): The outcome of combining precision and sensitivity. It is critical since better accuracy means reduced sensitivity, and vice versa. Equation (21) computes it.

$$F - \text{Score} = 2 * \frac{\text{precision} * \text{recall}}{\text{precision} + \text{recall}} \tag{21}$$

Additionally, the ability of each model to forecast groundwater salinity was evaluated using the Bayesian information criterion (BIC) and the AIC. The AIC is a technique to assess a model's capacity for value estimation or prediction. It is dependent on the sample data's goodness of fit. The BIC measures how well a model balances complexity and data representation accuracy. It adopts a similar strategy to the AIC. In this instance, the model with the lowest AIC and BIC values is the most beneficial. You can use the following equations to determine a model's AIC and BIC:

$$\text{AIC} = 2k - 2\log(L) \tag{22}$$

$$\text{BIC} = 2\log(n)k - 2\text{In}(L) \tag{23}$$

where L is the likelihood factor, n is the total number of sizes, and there are three definitions for k: it represents the total number of measurements, it stands for the total number of independent variables (where $k = 14$), and it denotes the total number of independent variables.

1. Precision

Figure 5 and Table 1 compare the precision of the BiLSTM-PMIS method to that of other methods already in use. The graph shows how the application of ML has improved performance precision. For instance, the BiLSTM-PMIS has a precision value of 97.753% for data 100, compared to accuracy values of 86.562, 88.527, 91.265, 94.736, and 96.725% for the KNN, KDE, LSTM, GRNN, and ANN models. The BiLSTM-PMIS model, however, excelled with various data sizes. Similar to this, for KNN, KDE, LSTM, GRNN, and ANN models, the precision value of BiLSTM-PMIS under 600 data is 96.057, 86.536, 89.852, 91.853, 93.625, and 96.224%, respectively.

2. Recall

Figure 6 and Table 2 compare the BiLSTM-PMIS and various recall methods. The graph demonstrates how ML has enhanced memory performance. For data 100, the recall values for the KNN, KDE, LSTM, GRNN, and ANN models are 83.763, 84.526, 85.938, 88.735, and 89.735%, respectively, whereas the recall value for the BiLSTM-PMIS model is 94.838%. But with different-sized data, the BiLSTM-PMIS model performed best. Similarly, the recall for the BiLSTM-PMIS is 97.735% with 600 data as opposed to the KNN, KDE, LSTM, GRNN, and ANN models, which have recall values of 83.974, 86.736, 87.735, 88.943, and 92.836%, respectively.

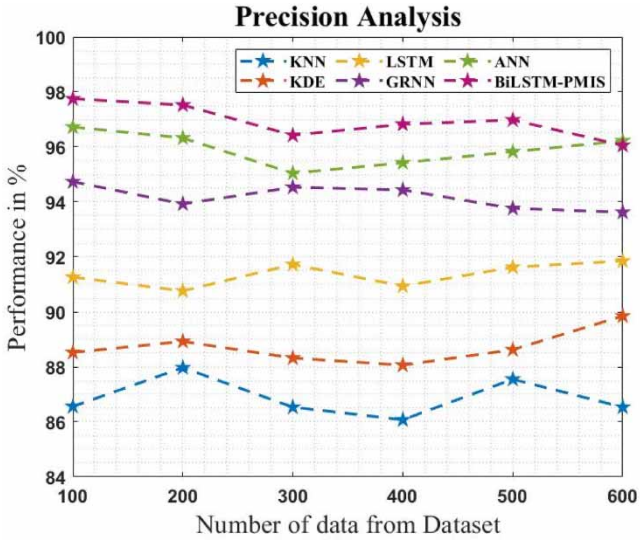

Figure 5 | Precision analysis for BiLSTM-PMIS method with existing systems.

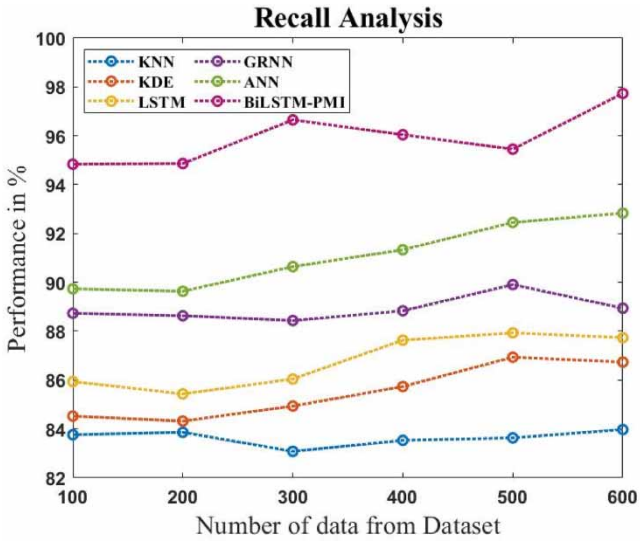

Figure 6 | Recall analysis for BiLSTM-PMIS method with existing systems.

3. *F*-score

In Figure 7 and Table 3, the BiLSTM-PMIS approach is compared to other *F*-scores techniques. The graph shows how ML improved the *F*-score's performance. BiLSTM-PMI has an *F*-score of 93.846% for the dataset, which is higher than that of the KNN, KDE, LSTM, GRNN, and ANN models, which have *F*-scores of 79.833, 84.937, 86.937, 89.224, and 92.836%, respectively. The BiLSTM-PMIS model has, however, shown that it performs better with different data sizes. The BiLSTM-PMIS model has an *F*-score value of 96.536% with 600 data, compared to the KNN, KDE, LSTM, GRNN, and ANN models, which have discounts of 84.437, 87.534, 88.673, 90.736, and 93.526%, correspondingly.

4. RMSE

An RMSE comparison of the BiLSTM-PMIS technique with many well-known approaches is shown in Figure 8 and Table 4. The graph demonstrates how ML was used to enhance performance while reducing RMSE. While the RMSE value for the BiLSTM-PMIS model is 28.843%, the RMSE values for the KNN, KDE, LSTM, GRNN, and ANN models

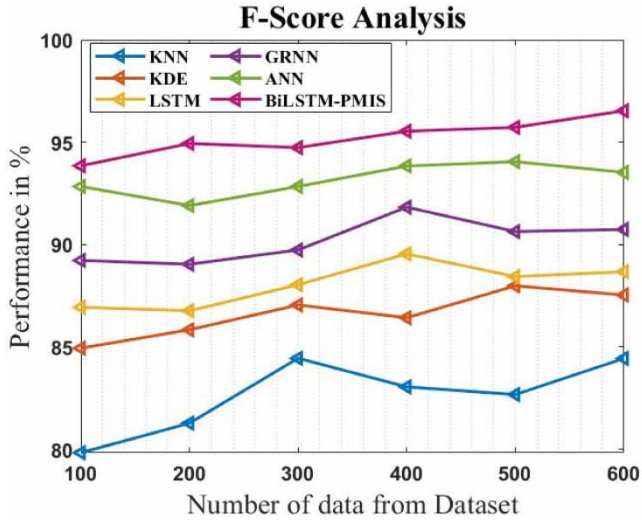

Figure 7 | *F*-score analysis for BiLSTM-PMIS method with existing systems.

Table 3 | *F*-score analysis for BiLSTM-PMIS method with existing systems

No of data from dataset	KNN	KDE	LSTM	GRNN	ANN	BiLSTM-PMIS
100	79.833	84.937	86.937	89.224	92.836	93.846
200	81.275	85.837	86.764	89.037	91.904	94.937
300	84.447	87.048	88.038	89.736	92.836	94.735
400	83.048	86.425	89.546	91.826	93.836	95.535
500	82.674	87.984	88.435	90.634	94.047	95.725
600	84.437	87.534	88.673	90.736	93.526	96.536

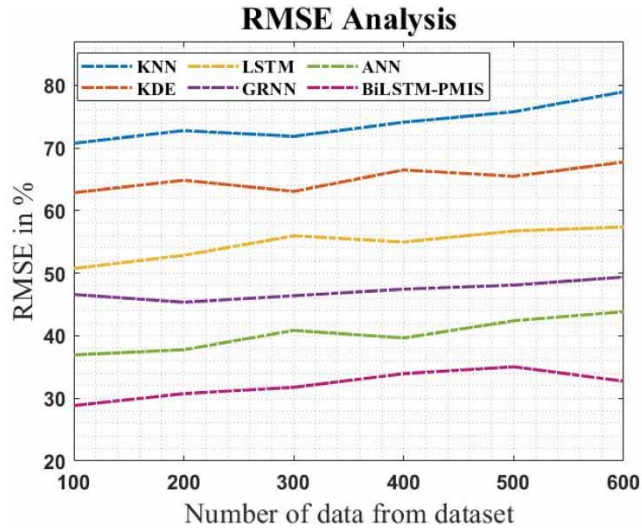

Figure 8 | RMSE analysis for BiLSTM-PMIS method with existing systems.

Table 4 | RMSE analysis for BiLSTM-PMIS method with existing systems

No of data from dataset	KNN	KDE	LSTM	GRNN	ANN	BiLSTM-PMIS
100	70.735	62.846	50.736	46.586	36.937	28.843
200	72.763	64.836	52.836	45.347	37.754	30.746
300	71.836	63.048	55.957	46.387	40.846	31.763
400	74.095	66.486	54.967	47.433	39.644	33.944
500	75.764	65.446	56.736	48.085	42.384	35.037
600	78.946	67.745	57.365	49.365	43.846	32.734

all only slightly improved to 70.735, 62.846, 50.736, 46.586, and 36.93%, respectively, using 100 data points. However, the BiLSTM-PMIS model has shown excellent performance for numerous datasets with low RMSE values. Comparable results for the KNN, KDE, LSTM, GRNN, and ANN models are, respectively, 70.735, 67.745, 57.365, 49.365, and 43.846%, but the BiLSTM-PMIS's RMSE value under 600 data points is 32.734%.

5. Akaike information criterion

Figure 9 and Table 5 display an AIC comparison of the BiLSTM-PMIS methodology and other current methodologies. The graph demonstrates how the performance of the ML technique increased with a lower AIC value. In contrast to slightly better AIC values for the KNN, KDE, LSTM, GRNN, and ANN models (843.84, 803.84, 749.68, and 633.76), the BiLSTM-PMIS model has an AIC value of 517.99 with data 100. However, the BiLSTM-PMIS model has been shown to perform the best across a range of data sizes with low AIC values. Similar to how BiLSTM-PMIS's AIC value is 1,054.87 under 600 data, KNN, KDE, LSTM, GRNN, and ANN models' AIC values are 1,583.93, 1,473.83, 1,333.73, 1,231.07, and 1,095.76, respectively.

6. Bayesian Information Criterion

Figure 10 and Table 6 display a BIC comparison of the BiLSTM-PMIS strategy and other widely used methods. The graph shows how, with a lower BIC value, the ML technique provided higher performance. The BiLSTM-PMIS model, for example, has a BIC value of 104.05 with data 100, whereas the BIC values for the KNN, KDE, LSTM, GRNN, and ANN models are marginally higher at 634.97, 536.57, 423.87, 309.25, and 236.86, respectively. However, the BiLSTM-PMIS model has been shown to perform at its best across a range of data sizes with low BIC values. BIC values for the KNN, KDE, LSTM, GRNN,

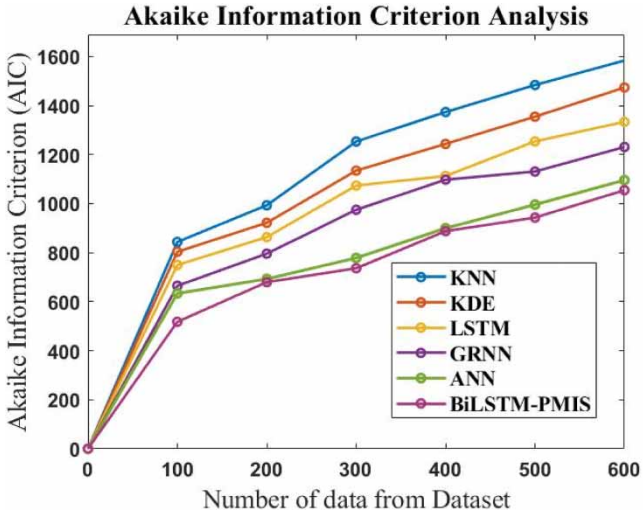

Figure 9 | Akaike information criterion analysis for BiLSTM-PMIS method with existing systems.

Table 5 | Akaike information criterion analysis for BiLSTM-PMIS method with existing systems

No of data from dataset	KNN	KDE	LSTM	GRNN	ANN	BiLSTM-PMIS
100	843.84	803.84	749.68	664.89	633.76	517.99
200	993.48	921.83	863.48	795.86	692.67	679.68
300	1,253.38	1,134.74	1,073.54	974.94	778.43	736.38
400	1,373.74	1,243.77	1,113.03	1,097.86	899.75	887.76
500	1,483.93	1,354.83	1,253.94	1,131.07	995.95	943.06
600	1,583.93	1,473.83	1,333.73	1,231.07	1,095.76	1,054.87

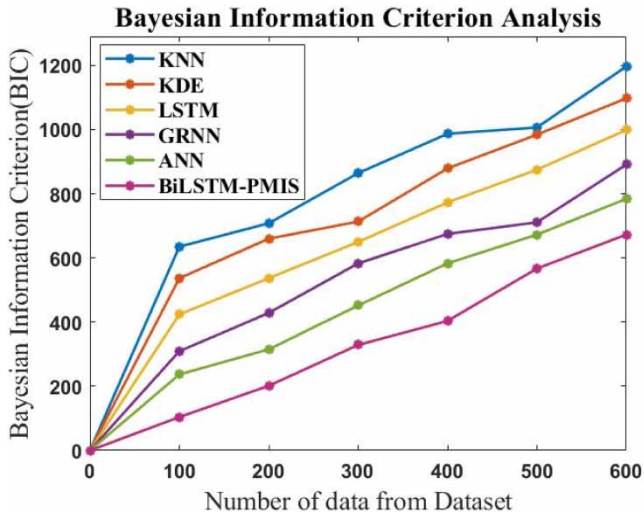

Figure 10 | Bayesian information criterion analysis for BiLSTM-PMIS method with existing systems.

Table 6 | Bayesian information criterion analysis for BiLSTM-PMIS method with existing systems

No of data from dataset	KNN	KDE	LSTM	GRNN	ANN	BiLSTM-PMIS
100	634.97	536.57	423.87	309.25	236.86	104.05
200	707.87	659.86	536.75	428.53	315.06	201.46
300	863.98	713.06	649.76	582.76	451.66	328.75
400	986.75	878.76	772.87	674.64	583.05	403.64
500	1,006.34	983.97	874.76	710.76	672.45	566.85
600	1,196.34	1,097.06	998.76	890.76	783.87	672.46

and ANN models are 1.196.34, 1.097.06, 998.76, and 783.87, respectively, whereas the BIC value of the BiLSTM-PMIS is 672.46 for 600 data.

7. Accuracy

In Figure 11 and Table 7, the accuracy of the BiLSTM-PMIS approach is compared to that of other current techniques. The graph demonstrates how ML algorithms have become more effective and accurate. The BiLSTM-PMIS model, for example, has an accuracy of 95.207% about data 100, compared to 93.563, 90.872, 88.735, 83.927, and 85.837% for the KNN, KDE,

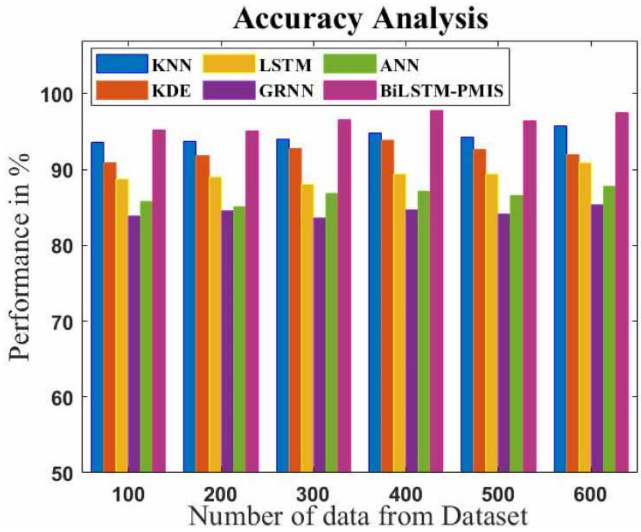

Figure 11 | Accuracy analysis for BiLSTM-PMIS method with existing systems.

Table 7 | Accuracy analysis for BiLSTM-PMIS method with existing systems

No of data from dataset	KNN	KDE	LSTM	GRNN	ANN	BiLSTM-PMIS
100	93.563	90.872	88.735	83.927	85.837	95.207
200	93.748	91.837	88.952	84.536	85.043	95.072
300	94.036	92.733	88.063	83.626	86.825	96.527
400	94.836	93.846	89.463	84.726	87.103	97.834
500	94.323	92.635	89.436	84.093	86.563	96.435
600	95.735	92.039	90.832	85.433	87.837	97.436

LSTM, GRNN, and ANN models. The BiLSTM-PMIS model has, however, been shown to perform better with various data sizes. In comparison to the BiLSTM-PMIS, which has an accuracy of 97.436% for 600 data from the dataset, the accuracy values for KNN, KDE, LSTM, GRNN, and ANN models are 95.735, 92.039, 90.832, 85.433, and 87.837%, respectively.

5. CONCLUSION

This paper compares contemporary ML methods for determining the factors affecting groundwater salinity. This study uses the representative DL model BiLSTM to forecast groundwater salinity. Recent studies have shown a significant finding in the area of time series modeling that has the community's interest. It has been observed that information-theoretic algorithms for selecting input variables, precisely the partial mutual information (PMI) selection (PMIS), offer a more accurate representation of the underlying process when compared to linear alternatives like PCIS, particularly in applications related to water resources, such as PCIS (Water Resources Planning, Construction, and Operation Management System). This research emphasizes the importance of using nonlinear techniques to capture the model's complexity and dynamism, which will improve our knowledge of water resource systems. For nonlinear variable input selection issues, PMIS is a well-liked algorithm in water resource modeling. Various sample combinations are made using the PMIS-selected predictors to train different BiLSTM models. When predicting groundwater levels, the anticipated values from several BiLSTM models are used to gauge the degree of uncertainty. To address groundwater salinity issues brought on by excessive groundwater use in coastal lowland areas, policymakers can use the findings to create remediation and management plans. Immediate action is imperative for the act to ensure sustainable groundwater management in coastal regions, given the significant impact of human-caused factors

on groundwater salinization. Overall, the BiLSTM-PMIS reduced the RMSE value is 32.734%, while it improved its precision value to 96.057%, recall value is 97.735%, *F*-score value is 96.536%, and accuracy value is 97.436%. In addition to accurately predicting groundwater levels, the BiLSTM also assessed the predictability of groundwater levels when paired with PMI and bootstrap. More research is necessary to improve GWL projections in various locations with complex climatic elements, such as coastal areas and subsurface reservoir management regions. To do this, it is advisable to examine state-of-the-art research techniques that employ hybrid models combining the wavelet transform, box–cox transformation, and BiLSTM models. Significant advancements in forecasting groundwater levels might be expected by using such approaches. However, it is essential to recognize that the ability to predict groundwater levels in dry areas still needs to be improved.

ACKNOWLEDGEMENT

The authors thank the Researchers Supporting Project number (RSP2023R407), King Saud University, Riyadh, Saudi Arabia for the financial support.

DATA AVAILABILITY STATEMENT

All relevant data are included in the paper or its Supplementary Information.

CONFLICT OF INTEREST

The authors declare there is no conflict.

REFERENCES

Al Jami, A., Himel, M. U., Hasan, K., Basak, S. R. & Mita, A. F. 2020 Narx neural network approach for the monthly prediction of groundwater levels in Sylhet Sadar, Bangladesh. *Journal of Groundwater Science and Engineering* **8** (2), 118–126.

Alotaibi, Y., Alghamdi, S., Khalafand, O. I. & Nanda, A. K. 2022 Improved metaheuristic-driven energy-aware cluster-based routing scheme for IoT-assisted wireless sensor networks. *Sustainability* **14**, 7712. https://doi.org/10.3390/su14137712.

Antonellini, M., Allen, D. M., Mollema, P. N., Capo, D. & Greggio, N. 2015 Groundwater freshening following coastal progradation and land reclamation of the Po Plain, Italy. *Hydrogeology Journal* **23**, 1009–1026.

Bidwell, V. J. 2005 Realistic forecasting of groundwater level, based on the eigenstructure of aquifer dynamics. *Mathematics and Computers in Simulation* **69** (1–2), 12–20.

Chen, C., He, W., Zhou, H., Xue, Y. & Zhu, M. 2020 A comparative study among machine learning and numerical models for simulating groundwater dynamics in the Heihe river basin, northwestern China. *Scientific Reports* **10** (1), 1–13.

Choubin, B. & Malekian, A. 2017 Combined gamma and M-test-based ANN and ARIMA models for groundwater fluctuation forecasting in semiarid regions. *Environmental EarthSciences* **76** (15), 1–10.

Colombani, N., Mastrocicco, M. & Giambastiani, B. M. S. 2015 Predicting salinization trends in a lowland coastal aquifer: Comacchio (Italy). *Water Resources Management* **29**, 603–618.

Cozzolino, D., Greggio, N., Antonellini, M. & Giambastiani, B. M. S. 2017 Natural and anthropogenic factors affecting freshwater lenses in coastal dunes of the Adriatic coast. *Journal of Hydrology* **551**, 804–818.

Daliakopoulos, I. N., Coulibaly, P. & Tsanis, I. K. 2005 Groundwater level forecasting using artificial neural networks. *Journal of Hydrology* **309** (1–4), 229–240.

Demirci, M., Üneş, F. & Körlü, S. 2019 Modeling of groundwater level using artificial intelligence techniques: a case study of Reyhanli region in Turkey. *Applied Ecology and Environmental Research* **17** (2), 2651–2663.

Derbela, M. & Nouiri, I. 2020 Intelligent approach to predict future groundwater level based on artificial neural networks (ANN). *Euro-Mediterranean Journal for Environmental Integration* **5** (3), 1–11.

Giambastiani, B. M. S., Macciocca, V. R., Molducci, M. & Antonellini, M. 2020 Factors affecting water drainage long-time series in the salinized low-lying coastal area of Ravenna (Italy). *Water* **12**, 256.

Guzman, S. M., Paz, J. O. & Tagert, M. L. M. 2017 The use of NARX neural networks to forecast daily groundwater levels. *Water Resources Management* **31** (5), 1591–1603.

Guzman, S. M., Paz, J. O., Tagert, M. L. M. & Mercer, A. E. 2019 Evaluation of seasonally classified inputs for the prediction of daily groundwater levels: Narx networks vs support vector machines. *Environmental Modeling & Assessment* **24** (2), 223–234.

Huang, F., Huang, J., Jiang, S. H. & Zhou, C. 2017 Prediction of groundwater levels using evidence of chaos and support vector machine. *Journal of Hydroinformatics* **19** (4), 586–606.

Iqbal, M., Naeem, U. A., Ahmad, A., Ghani, U. & Farid, T. 2020 Relating groundwater levels with meteorological parameters using ANN technique. *Measurement* **166**, 108163.

Javadinejad, S., Dara, R. & Jafary, F. 2020 Modelling groundwater level fluctuation in an Indian coastal aquifer. *Water SA* **46** (4), 665–671.

Lee, S.-I., Lee, S.-K. & Hamm, S.-Y. 2009 A model for groundwater time-series from the well field of riverbank filtration. *Journal of Korea Water Resources Association* **42** (8), 673–680.

Maroufpoor, E., Jalali, S., Nikmehr, M., Shiri, S., Shiri, N. & Maroufpoor, J. 2020 Modeling groundwater quality by using hybrid intelligent and geostatistical methods. *Environmental Science and Pollution Research* **27** (22), 28183–28197.

Metwally, A. M., Santhamoorthy, M. & Satyanarayana Gupta, M. 2022 Metaheuristics with deep transfer learning enabled detection and classification model for industrial waste management. *Chemosphere* **308**, 136046. https://doi.org/10.1016/j.chemosphere.2022.136046.

Mosavi, A., Sajedi Hosseini, F., Choubin, B., Taromideh, F., Ghodsi, M., Nazari, B. & Dineva, A. A. 2021b Susceptibility mapping of groundwater salinity using machine learning models. *Environmental Science and Pollution Research* **28** (9), 10804–10817.

Neumann, B., Ott, K. & Kenchington, R. 2017 Strong sustainability in coastal areas: a conceptual interpretation of SDG 14. *Sustainability Science* **12**, 1019–1035.

Nie, S., Bian, J., Wan, H., Sun, X. & Zhang, B. 2017 Simulation and uncertainty analysis for groundwater levels using radial basis function neural network and support vector machine models. *Journal of Water Supply: Research and Technology – AQUA* **66** (1), 15–24.

Post, V. E. A., Eichholz, M. & Brentführer, R. 2018 *Groundwater Management in Coastal Zones*. Bundesanstalt für Geowissenschaften und Rohstoffe (BGR), Hannover, Germany, p. 107.

Pourghasemi, H. R., Sadhasivam, N., Yousefi, S., Tavangar, S., Ghaffari Nazarlou, H. & Santosh, M. 2020 Using machine learning algorithms to map the groundwater recharge potential zones. *Journal of Environmental Management* **265**, 110525.

Prakash, M., Geetha, B. T., Asha, S. M. R. & Roberts, M. K. 2022 Artificial humming bird with data science enabled stability prediction model for smart grids. *Sustainable Computing: Informatics and Systems* **36**, 1–10. https://doi.org/10.1016/j.suscom.2022.100821.

Sadat-Noori, M., Glamore, W. & Khojasteh, D. 2020 Groundwater level prediction using genetic programming: the importance of precipitation data and weather station location on model accuracy. *Environmental Earth Sciences* **79**, 37.

Sahoo, S. & Jha, M. K. 2015 On the statistical forecasting of groundwater levels in unconfined aquifer systems. *Environmental Earth Sciences* **73** (7), 3119–3136.

Shamsuddin, M. K. N., Kusin, F. M., Sulaiman, W. N. A., Ramli, M. F., Baharuddin, M. F. T. & Adnan, M. S. 2017 Forecasting of groundwater level using artificial neural network by incorporating river recharge and river bank infiltration. In *MATEC Web of Conferences*. Vol. 103, EDP Sciences, p. 04007.

Sharafati, A., Asadollah, S. B. H. S. & Neshat, A. 2020 A new artificial intelligence strategy for predicting the groundwater level over the Rafsanjan aquifer in Iran. *Journal of Hydrology* **591**, 125468.

Sun, A. Y., Scanlon, B. R., Zhang, Z., Walling, D., Bhanja, S. N., Mukherjee, A. & Zhong, Z. 2019 Combining physically based modeling and deep learning for fusing GRACE satellite data: can we learn from mismatch? *Water Resources Research* **55** (2), 1179–1195.

Sunayana, K., Kalawapudi, O. & Dube Sharma, R. 2020 Use of neural networks and spatial interpolation to predict groundwater quality. *Environment, Development and Sustainability* **22** (4), 2801–2816. doi:10.1007/s10668-019-00319-2.

Vu, M., Jardani, A., Massei, N. & Fournier, M. 2020 Reconstruction of missing groundwater level data by using long short-term memory (LSTM) deep neural network. *Journal of Hydrology* **597**, 125776.

Yaseen, Z. M., Mohtar, W. H. M. W., Ameen, A. M. S., Ebtehaj, I., Razali, S. F. M., Bonakdari, H., Salih, S. Q., Al-Ansari, N. & Shahid, S. 2019 Implementation of univariate paradigm for streamflow simulation using hybrid data-driven model: a case study in tropical region. *IEEE Access* **7**, 74471–74481.

Yousefi, H., Zahedi, S., Niksokhan, M. H. & Momeni, M. 2019 Ten-year prediction of groundwater level in Karajplain (Iran) using MODFLOW2005-NWT in MATLAB. *Environmental Earth Sciences* **78** (12), 343.

First received 25 May 2023; accepted in revised form 2 August 2023. Available online 14 August 2023